J. Fluid Mech. (1995), *vol.* 292, *pp.* 249–270

Effect of islands upon dispersion in rivers

By RONALD SMITH

Department of Mathematical Sciences, Loughborough University of Technology, Loughborough, LE11 3TU, UK

(Received 15 June 1994 and in revised form 18 January 1995)

A general formulation is given for the dispersion of conservative tracers in steady flow in multi-connected channels. A multi-index is used to distinguish the different routes for tracer between the source and the observation position. For each route exact formulae are obtained for the time integral, time centroid, and cross-channel average of the temporal variance. The total concentration is the superposition of the contributions from the different routes.

1. Introduction

It takes the order of a hundred channel breadths downstream for a point release of conservative tracer to become well mixed across a river (Yotsukura & Sayre 1976). Consequently, there is a substantial stretch of river in which the concentrations are strongly dependent upon the precise position of release (Smith 1981). Similarly, the rate of dilution at one section of a river depends upon the upstream geometry over distances which can encompass several river bends (Fischer 1969). Over such large lengthscales there can be additional complications such as deltas, tributaries or islands.

Daish (1985) investigated the effect of single and repeated splitting of a flow. He showed that it is only far downstream that the rate of dilution ceases to be dominated by conditions prior to the splitting. Thus, the assumption of 'perfectly mixing vertices' invoked in earlier mathematical investigations (Saffman 1969; Ultman & Blatman 1977; Adler 1985) is quite inappropriate for rivers. Smith & Daish (1991) investigated the effect of a 'clean' tributary on the dilution process. They interpreted junctions as being a special form of initial conditions. For conservative tracer released far upstream of a river junction, they showed that in addition to dilution by the 'clean' water, there could be substantial effects upon the time-of-travel and the temporal spread of the concentration as observed far downstream of the junction.

The purpose of the present work is to give a generalized mathematical analysis which encompasses branching and re-joining (deltas and islands). The concentration is decomposed into contributions associated with distinct routes around any islands. Each contribution evolves in an essentially diffusive manner and is quantified in terms of the dosage, time-of-travel and spread. However, the superposition could be non-diffusive in character and exhibit features such as multiple concentration peaks.

On flood plains there can be distinct river routes which rejoin many kilometres downstream. In earlier centuries, after the floods in the rainy season, all but one of the routes could be expected to silt up (it would not always be the same route that would persist). Now that river water is used for the irrigation of adjacent farmland, in industry and for recreation, remedial action would be taken to keep any useful river branches flowing. Another category of multiple routes occurs when a navigation canal cuts across a lengthy bend or series of bends. Local examples in the East Midlands of

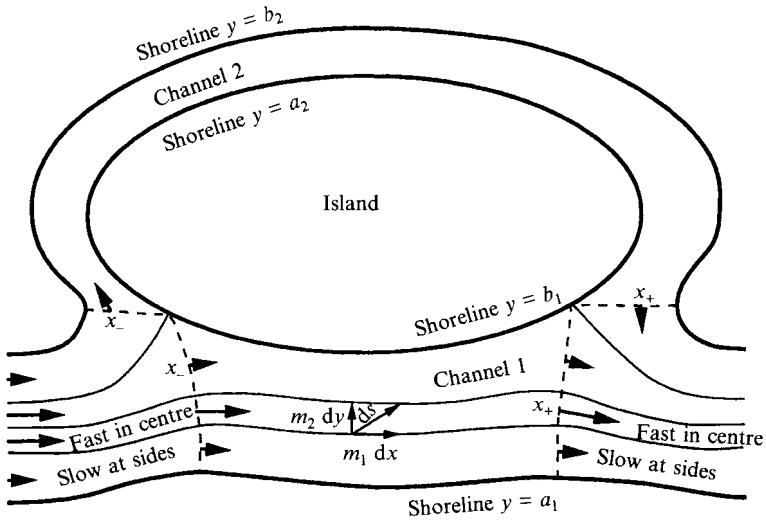

FIGURE 1. Coordinates aligned along and across the flow.

the UK are the River Trent, the Old Trent and the Trent-Mersey canal. Hence, on flood plains 'islands' can be exceedingly long.

2. Flow-following coordinate system

It only takes of the order of 40 water depths downstream for a tracer to become vertically well-mixed. In practice (except for dredged channels) this is much less than the horizontal lengthscales of major topographical features such as islands. For a modest sized river of depth 1 m, this horizontal lengthscale for vertical mixing would be 40 m. So, we can make the simplification of considering the vertically averaged concentration as advected along in the vertically averaged flow.

If the flow is steady, then it is also convenient to use an orthogonal coordinate system (x, y) aligned along and across the flow (Yotsukura & Sayre 1976). To allow for the different flow distances either side of islands and for the varying separation between adjacent flow lines, we have non-constant metric coefficients $m_1(x, y)$, $m_2(x, y)$ (see figure 1). In terms of the metric coefficients, the physical distance ds associated with small coordinate displacements (dx, dy) is given by the Pythagorean formula

$$ds^2 = m_1^2\,dx^2 + m_2^2\,dy^2. \tag{2.1}$$

At points where the flow divides or re-joins, the longitudinal coordinate x is assumed to be adjusted (by increasing m_1 in the long channels) so that there is a single value of x. Any shorelines are streamlines with $y =$ constant. At a fixed value of x we use an index i to label the channels and we designate the y-coordinates of the shorelines as a_i, b_i. At separation or joining points we could re-designate the y-labelling of the streamlines provided that we ensured that the concentration was correctly matched across the change of labelling.

The alignment of the coordinate system with the flow means that there is only a single non-zero velocity component $m_1 u_1$, where $u_1(x, y)$ is the rate-of-crossing of x-contours. For a steady flow, the conservation-of-mass equation is

$$\partial_x(m_1 m_2 h u_1) = 0, \tag{2.2}$$

where $h(x, y)$ is the water depth.

The advection–diffusion equation for the conservative tracer concentration $c(x, y, t)$ is

$$m_1 m_2 h[\partial_t c + u_1 \partial_x c] - \partial_y\{(m_1/m_2) h\kappa \partial_y c\} = q\delta(x-x_0)\,\delta(y-y_0)\,\delta(t-t_0). \quad (2.3)$$

Here $\kappa(x, y)$ is the transverse diffusion coefficient, which via vertical averaging encompasses the shear dispersion associated with any secondary circulation (Fischer 1969). The source strength is q and the delta functions δ signify the source position $x_0 y_0$ and timing t_0. Longitudinal diffusion has been ignored because the implicit lengthscale is of order 100 channel breadths, so ∂_x^2 terms are of order 10^{-4} relative to ∂_y^2 terms. The condition of no loss of tracer through shorelines is

$$h\kappa \partial_y c = 0 \quad \text{on} \quad y = a_i, b_i. \quad (2.4)$$

3. Pollution via many routes

When there are islands there can be more than one route for the tracer to get from the point of discharge (x_0, y_0) to the present point of observation (x, y). The pollution contributions from the different routes can have quite dissimilar magnitudes, times-of-travel, and temporal spreads. Indeed, a complicated-looking superposition could be composed of individually simple parts. Thus, it is desirable to distinguish between the multiple contributions.

If at n successive junctions the selection of channel is $i_1, i_2, \ldots, i_n$ then we can use the multi-index

$$\boldsymbol{\mu} = i_1, \ldots, i_n \quad (3.1)$$

to label the corresponding contribution $c_{\mu}(x, y, t; x_0, y_0, t_0)$ to the concentration. Different routes can involve different numbers of junctions and so can have different lengths for the multi index $\boldsymbol{\mu}$. Along the designated route, c_{μ} satisfies the advection–diffusion equation (2.3) and the boundary conditions (2.4). However, any tracer that enters a channel which is not part of the designated route (a 'non-designated' channel) is subsequently ignored because it is accounted for in another route. In particular, at the downstream end of a non-designated channel c_{μ} is zero.

4. The dosage

Soon after Taylor's (1953) pioneering work on shear dispersion, Aris (1956) developed a systematic mathematical procedure for calculating the spatial moments of the concentration distribution in plane parallel flows. The successive moments give more and more detailed information about the spatial concentration profile. In particular, the rate of dilution is conventionally characterized in terms of the halved growth rate of the second moment (the shear dispersion coefficient). For rivers the longitudinal non-uniformity makes spatial moments inappropriate. However, temporal moments can be used instead (Tsai & Holley 1978, 1980; Smith 1984). From the concentration component $c_{\mu}(x, y, t; x_0, y_0, t_0)$ we define temporal moments relative to a reference time-of-travel $\tau_{\mu}(x; x_0, y_0)$:

$$c_{\mu}^{(j)} = \int_{-\infty}^{\infty} (t - \tau_{\mu} - t_0)^j c_{\mu}(x, y, t)\,\mathrm{d}t \quad (j = 0, 1, \ldots). \quad (4.1)$$

The specification of τ_{μ} is an important aspect of the subsequent analysis.

The zero moment $c_{\mu}^{(0)}(x, y; x_0, y_0)$ is the dosage: the time-integrated concentration experienced at the location (x, y) for the particular route $\boldsymbol{\mu}$. To remove the proportionality to the source strength q we write

$$c_{\mu}^{(0)} = q\Phi_{\mu}(x, y; x_0, y_0). \quad (4.2)$$

At junctions the continuity of concentration implies that Φ_μ is likewise continuous. Also, the diffusion equation (2.3) for c gives rise to a corresponding equation for Φ_μ:

$$m_1 m_2 h u_1 \partial_x \Phi_\mu - \partial_y\{(m_1/m_2) h\kappa \partial_y \Phi_\mu\} = \delta(x-x_0)\,\delta(y-y_0), \tag{4.3a}$$

with
$$h\kappa \partial_y \Phi_\mu = 0 \quad \text{on shorelines,} \tag{4.3b}$$

and
$$\Phi_\mu = 0 \quad \text{at exit from non-designated channels.} \tag{4.3c}$$

the multi-index $\mu = i_1, \ldots, i_n$ labels the designated channels (up to and including the present channel $i = i_n$). The value of Φ_μ can only be influenced by the upstream route and not by the subsequent selection of branches.

Within the i channel the cross-stream integral

$$\theta_\mu(x_0, y_0) = \int_{a_i}^{b_i} m_1 m_2 h u_1 \Phi_\mu \,\mathrm{d}y \tag{4.4}$$

is constant (independent of x) and measures the fraction of the original discharge that has traversed the route $\mu = i_1, \ldots, i_n$ into the $i = i_n$ channel. The sum of the θ_μ over all routes and channels up to the present value of x, accounts for all the original discharge:

$$\sum_\mu \theta_\mu = 1. \tag{4.5}$$

The diffusive character of (4.3a) and the non-negative forcing ensures that Φ_μ is non-negative. A natural cross-channel average value associated with the route μ involves the weight factor $m_1 m_2 h u_1 \Phi_\mu$:

$$[f]_\mu = \frac{1}{\theta_\mu} \int_{a_i}^{b_i} m_1 m_2 h u_1 \Phi_\mu f \,\mathrm{d}y. \tag{4.6}$$

If a channel remains distinct, then sufficiently far downstream (100 channel breadths) the function Φ_μ becomes constant. The asymptotic uniform value is the quotient of the flux of tracer into that channel and the flux of water along that channel:

$$\Phi_\mu \sim \theta_\mu \Big/ \int_{a_i}^{b_i} m_1 m_2 h u_1 \,\mathrm{d}y. \tag{4.7}$$

For example, far downstream of a river junction it is the increased flux of water that dilutes the eventual dosage (Smith & Daish 1991). Also, far downstream the average $[f]_\mu$ becomes the same as a flux-weighted average (Smith 1984).

A total dosage $c^{(0)}$ at an observation position (x, y) in channel i can be obtained by a summation over all possible routes into that channel of the component dosage $c_\mu^{(0)}$:

$$c^{(0)} = q \sum_\mu \Phi_\mu. \tag{4.8}$$

5. Time-of-travel

At different observation positions y across the ith channel the precise time of arrival will differ from the reference time-of-travel $\tau_\mu(x; x_0, y_0)$. Thus, we write

$$c_\mu^{(1)} = q \Phi_\mu G_\mu. \tag{5.1}$$

Within a channel the time-of-arrival function $G_\mu(x, y; x_0, y_0)$ satisfies the equations

$$m_1 m_2 h u_1 \partial_x(\Phi_\mu G_\mu) - \partial_y\{(m_1/m_2) h\kappa \partial y(\Phi_\mu G_\mu)\} = m_1 m_2 h \Phi_\mu 1 - u_1(\mathrm{d}\tau_\mu/\mathrm{d}x), \tag{5.2a}$$

with $$h\kappa\,\partial y(\Phi_\mu G_\mu) = 0 \quad \text{on shorelines,} \tag{5.2b}$$

and $$\Phi_\mu G_\mu = 0 \quad \text{at exit from non-designated channels.} \tag{5.2c}$$

To avoid systematic growth in G_μ it is appropriate to choose the reference time-of-travel to be

$$\tau_\mu(x; x_0, y_0) = \int_{x_0}^{x} \frac{\mathrm{d}x'}{\mathscr{U}_\mu(x'; x_0, y_0)}, \tag{5.3a}$$

with $$\frac{1}{\mathscr{U}_\mu(x; x_0, y_0)} = \frac{1}{\theta_\mu}\int_{a_i}^{b_i} m_1 m_2 h \Phi_\mu \,\mathrm{d}y. \tag{5.3b}$$

The reciprocal speed $1/\mathscr{U}_\mu$ is sometimes called the 'slowness'. If a channel is sufficiently long that Φ_μ becomes constant, then $\mathscr{U}_\mu$ eventually corresponds to travel at the bulk velocity for that channel.

The selection (5.3*a*, *b*) for the reference time-of-travel τ_μ ensures that

$$[G_\mu]_\mu = \text{constant along channel } i. \tag{5.4}$$

The constant can be incremented at a flow division if on average late-arriving fluid goes into the ith channel (Daish 1985). For a sufficiently long channel the departure from the average

$$\tilde{G}_\mu = G_\mu - [G_\mu]_\mu \tag{5.5}$$

becomes independent both of the route μ and of the source position (x_0, y_0).

A flux-weighted travel time summed over all routes and channels up to the present value of x

$$\tau(x; x_0, y_0) = \sum_\mu \theta_\mu(x_0, y_0)\, \tau_\mu(x; x_0, y_0) \tag{5.6}$$

corresponds to a flux-weighted slowness

$$\frac{1}{\mathscr{U}(x; x_0, y_0)} = \sum_\mu \frac{\theta_\mu(x_0, y_0)}{\mathscr{U}_\mu(x; x_0, y_0)}. \tag{5.7}$$

6. Temporal variance

In terms of the first few moments, the temporal variance $\sigma_\mu^2(x, y; x_0, y_0)$ is defined

$$\sigma_\mu^2 = \frac{c_\mu^{(2)}}{c_\mu^{(0)}} - \left(\frac{c_\mu^{(1)}}{c_\mu^{(0)}}\right)^2. \tag{6.1}$$

The second term in this definition takes account of the fact that the tracer arrives at different times at different places across the flow. The equation satisfied by the product $\Phi_\mu \sigma_\mu^2$ is

$$m_1 m_2 h u_1\, \partial_x(\Phi_\mu \sigma_\mu^2) - \partial_y\{(m_1/m_2)\, h\kappa\, \partial_y(\Phi_\mu \sigma_\mu^2)\} = 2(m_1/m_2)\, h\kappa\, \Phi_\mu (\partial_y G_\mu)^2, \tag{6.2a}$$

with $$h\kappa\, \partial_y(\Phi_\mu \sigma_\mu^2) = 0 \quad \text{on shorelines,} \tag{6.2b}$$

and $$\Phi_\mu \sigma_\mu^2 = 0 \quad \text{at exit from non-designated channels.} \tag{6.2c}$$

Downstream of the source x_0, the forcing term in (6.2*a*) is positive. Hence, downstream of x_0, the temporal variance σ_μ^2 is likewise positive.

When integrated across the ith channel, (6.2*a*) yields the result

$$\theta_\mu \frac{\mathrm{d}}{\mathrm{d}x}[\sigma_\mu^2]_\mu = 2\int_{a_i}^{b_i} \frac{m_1}{m_2} h\kappa \Phi_\mu (\partial_y G_\mu)^2 \,\mathrm{d}y. \tag{6.3}$$

The integrand on the right-hand side is non-negative. Thus, on average σ_μ^2 increases downstream and we can define a positive-definite shear dispersion coefficient (Smith 1984):

$$\mathscr{D}_\mu(x; x_0, y_0) = \frac{\mathscr{U}_\mu^3}{\theta_\mu} \int_{a_i}^{b_1} \frac{m_1}{m_2} h\kappa \Phi_\mu (\partial_y G_\mu)^2 \, \mathrm{d}y. \tag{6.4}$$

The $\mathscr{U}_\mu^3$ factor arises because traditionally dispersion is quantified in terms of spatial rather than temporal variance. For a sufficiently long channel $\mathscr{D}_\mu$ becomes independent both of the route μ into that channel and of the source position (x_0, y_0). An alternative expression for the growth rate of $[\sigma_\mu^2]_\mu$, which avoids numerically awkward y-derivatives, is

$$\frac{\mathrm{d}}{\mathrm{d}x}[\sigma_\mu^2]_\mu = \frac{2}{\theta_\mu} \int_{a_i}^{b_i} m_1 m_2 h \Phi_\mu \tilde{G}_\mu \, \mathrm{d}y - \frac{\mathrm{d}}{\mathrm{d}x}[\tilde{G}_\mu^2]_\mu, \tag{6.5a}$$

where

$$\tilde{G}_\mu = G_\mu - [G_\mu]_\mu. \tag{6.5b}$$

From the temporal variance σ_μ^2 for each individual route μ we can construct a second moment for the superposition concentration (relative to the flux-weighted travel time τ):

$$\begin{aligned} c^{(2)} &= \int_{-\infty}^{\infty} (t-\tau-t_0)^2 \sum_\mu c_\mu \, \mathrm{d}t \\ &= \sum_\mu \int_{-\infty}^{\infty} \{(t-\tau_\mu-G_\mu-t_0)^2 + 2(\tau_\mu+G_\mu-\tau)(t-\tau_\mu-G_\mu-t_0) + (\tau_\mu+G_\mu-\tau)^2\} c_\mu \, \mathrm{d}t \\ &= \sum_\mu \Phi_\mu \sigma_\mu^2 + \sum_\mu (\tau_\mu+G_\mu-\tau)^2 \Phi_\mu. \end{aligned} \tag{6.6}$$

The flux-weighted concentration (summed over all routes and channels) has a temporal variance

$$s^2(x; x_0, y_0) = \sum_\mu \theta_\mu [\sigma_\mu^2]_\mu + \sum_\mu \theta_\mu [G_\mu^2]_\mu + \sum_\mu (\tau_\mu - \tau)^2 \theta_\mu. \tag{6.7}$$

The summation of $[\sigma_\mu^2]_\mu$ can be thought of as being a genuine measure of the shear dispersion process. The summation of $[G_\mu^2]_\mu$ involves temporal smearing across the flow associated with the time-of-arrival G_μ at different places across the flow. It is this contribution to s^2 that is associated with the apparent contraction in size of the tracer cloud when there is a sudden mean-square reduction in G_μ (Fukuoka & Sayre 1973; Smith 1984; Daish 1985). The summation of $(\tau_\mu - \tau)^2$ accommodates the different travel times for the different routes.

7. Cosine velocity and diffusivity profiles

In practice the equations (4.3), (5.2), (6.2) for the dosage, time-of-arrival and temporal variance would have to be solved numerically. Tsai & Holley (1978) noted that if a channel did not vary along its length then eigenfunction expansions could be used. For a laminar plane Poiseuille flow Daish (1985) numerically calculated the eigenfunctions. Here we use an example in which the eigenfunctions are orthogonal polynomials. The channels have $m_1 = 1$, constant depth H_i and cosine profiles of both velocity and diffusivity:

$$u_1(Y) = \tfrac{1}{2}\pi U_i \cos(\pi Y/2B_i), \quad \kappa = \tfrac{1}{2}\pi K_i \cos(\pi Y/2B_i). \tag{7.1a, b}$$

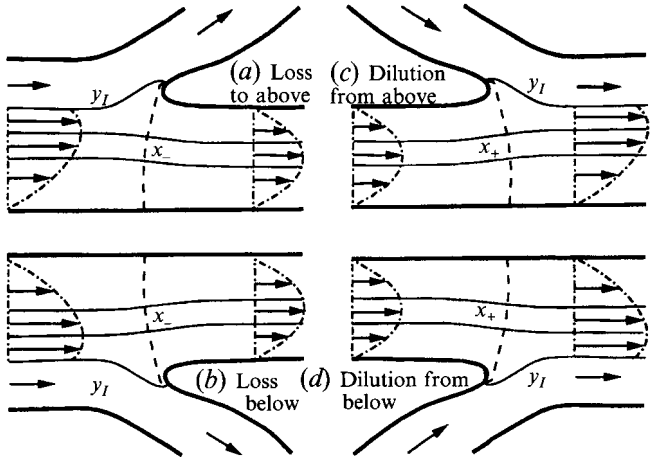

FIGURE 2. Four categories of junction (*a–d*).

Here Y is the physical distance from the centre of the ith channel, B_i is the distance from the centre to the sides, U_i is the bulk velocity and K_i is the mean transverse diffusivity.

A physical interpretation of the flow could be as a channel of constant depth with a non-uniform distribution of vegetation, which causes reduced flow and mixing towards the sides. In each individual channel the total volume flux of water is

$$Q_i = 2H_i U_i B_i. \tag{7.2}$$

The e-folding distance for the decay of symmetric non-uniformities in concentration is

$$L_e = \frac{2B_i^2 U_i}{3\pi^2 K_i} = \frac{B}{3\pi^2}\left(\frac{Q_i}{HK_i}\right). \tag{7.3}$$

For rivers, the quotient $(Q_i/H_i K_i)$ is typically about 6000, given an e-folding distance L_e of about $200B$. For antisymmetric non-uniformities the e-folding distance is a factor of three longer, i.e. about $600B$. As a reference case, for a modest sized river with half-width $B = 10$ m the principal e-folding distance L_e is 2 km and asymmetries take 6 km to decay.

As advocated by Yotsukura & Cobb (1972), we adjust the metric coefficient m_2 across the flow so that y-increments correspond to fractional volume flux increments across the channel:

$$m_2 = \frac{2B_i}{\pi}\sec\left(\frac{\pi Y}{2B_i}\right), \quad y = \sin\left(\frac{\pi Y}{2B}\right). \tag{7.4a, b}$$

Hence, in terms of y the cosine profiles (7.1 *a*, *b*) become square roots:

$$u_1(y) = \tfrac{1}{2}\pi U_i(1-y^2)^{1/2}, \quad \kappa = \tfrac{1}{2}\pi K_i(1-y^2)^{1/2}, \quad m_2 = \frac{2B}{\pi(1-y^2)^{1/2}}. \tag{7.5a–c}$$

At a flow division or junction (e.g. upstream or downstream ends of an island) we assume that the river geometry and flow adjust on a lengthscale short relative to that of lateral exchange (i.e. adjustment on a lengthscale comparable with one channel breadth rather than 100 breadths, in the reference case 20 m not 2 km). Thus, the matching of the concentration, dosage, time-of-arrival or temporal variance merely requires the correct identification of flow lines from one channel to another. The flow

line y_* in the i_*th channel is the downstream extension of y in the ith channel if the accumulated volume fluxes across the many channels match correctly:

$$\sum_{j=1}^{i-1} Q_j + \tfrac{1}{2}Q_i(1+y) = \sum_{j_*=1}^{i_*-1} Q_{j_*} + \tfrac{1}{2}Q_{i_*}(1+y_*). \tag{7.6}$$

hence, the re-designation of the y-labelling is linear.

Figure 2 illustrates the four elementary types of junction that can be encountered along a route: loss of solute to an upper/lower branch or dilution from an upper/lower tributary. Any more complicated type of junction (such as splitting into three) can be interpreted as being two or more of these elementary junctions very close together.

8. Matching Legendre series

In terms of the fractional volume flux coordinate (7.4*b*), the equation (4.3*a*) for the dosage now becomes

$$\tfrac{1}{2}Q_i\left[\partial_x \Phi_\mu - \frac{\pi^2 K_i}{4B_i^2 U_i}\partial_y((1-y^2)\partial_y \Phi_\mu)\right] = \delta(x-x_0)\,\delta(y-y_0). \tag{8.1}$$

The solution can be written as a Legendre polynomial expansion:

$$\Phi_\mu(x,y;x_0,y_0) = \sum_{n=0}^{\infty} \exp\left(-\frac{n(n+1)\pi^2 K_i}{4B_i^2 U_i}(x-\hat{x})\right)(2n+1)\,P_n(y)\,\hat{\Phi}_\mu^{(n)}(x_0,y_0). \tag{8.2}$$

Here the weight factors $\hat{\Phi}_\mu^{(n)}(x_0,y_0)$ are the values of the Legendre coefficients at the position $\hat{x}$, which can either be the source location x_0 or the start of the present channel (as specified in the final term in the multi-index $\boldsymbol{\mu}$). At the source the initial weight factors are

$$\hat{\Phi}^{(n)} = P_n(y_0)/Q_0. \tag{8.3}$$

The exponential decay term for $n = 2$ gives rise to the formula (7.3) for the e-folding distance.

At the end of a section of channel we need to ensure matching of Φ_μ into the next designated channel on the extended route. To do this we need to represent a Legendre polynomial $P_n(y)$ for the parent ith channel as a Legendre series for the next generation i_*th channel:

$$(2n+1)\,P_n(y) = \sum_{m=0}^{\infty} A_m^{(n)}(2m+1)\,P_m(y_*), \tag{8.4}$$

where the values y and y_* are linearly related via the volume flux matching (7.6). The coefficients $A_m^{(n)}$ are given by integrals

$$A_m^{(n)} = \frac{1}{2}\int_{y_*^{(-)}}^{y_*^{(+)}} (2n+1)\,P_n(y)\,P_m(y_*)\,\mathrm{d}y_* = \frac{Q_i}{2Q_{i_*}}\int_{y^{(-)}}^{y^{(+)}} (2n+1)\,P_n(y)\,P_m(y_*)\,\mathrm{d}y, \tag{8.5}$$

where the range of integration $(y_*^{(-)}, y_*^{(+)})$ or $(y^{(-)}, y^{(+)})$ is constrained so that only water that goes from i to i_* is involved. Conveniently, over the restricted range $P_n(y)$ and $P_m(y_*)$ are polynomials in y_* (or in y). Hence, a high-order Gauss numerical quadrature formula (Legendre weights and positions on the restricted range) gives exact results for $m+n$ up to twice that high order. In the special case in which all the water in channel i_* comes from channel i, the polynomial character of $P_n(y)$ over the full range $(-1, 1)$ of y_* ensures that the $A_m^{(n)}$ coefficients are zero for $m > n$.

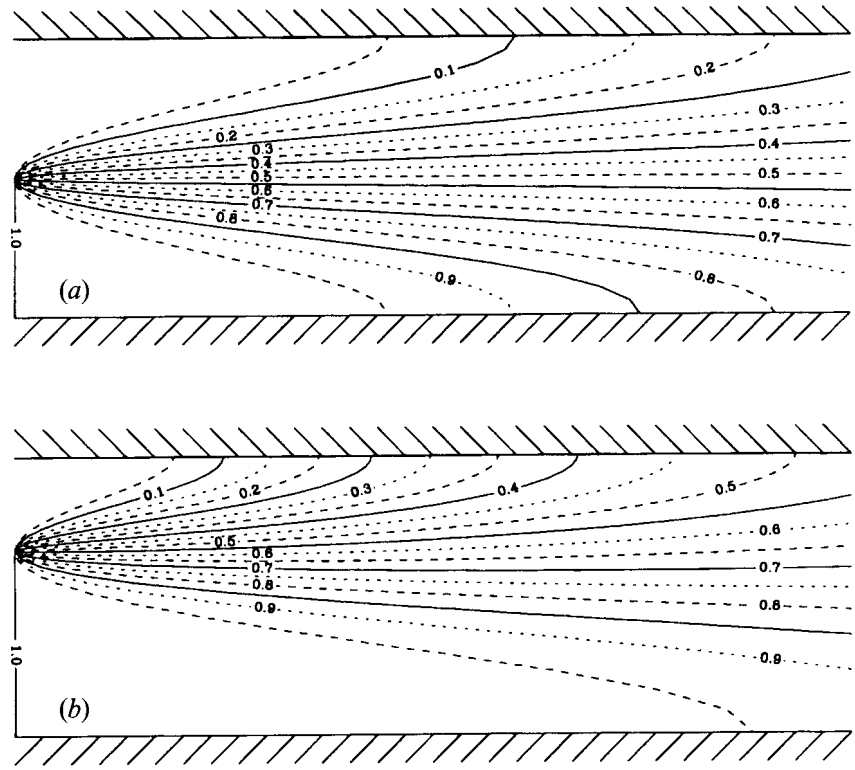

FIGURE 3. Contours of dosage for the lower route past an isolated island. Three (symmetric) e-folding distances downstream are shown. There is a foreshortening by a factor of about 100. (*a*) $y_I = 0$, (*b*) $y_I = 0.5$.

If the length of the parent channel (possibly starting at the source x_0) is L_i, then the weight factors $\hat{\Phi}^{(m)}_{\mu_*}(x_0, y_0)$ at the start of the next generation channel are

$$\hat{\Phi}^{(m)}_{\mu_*}(x_0, y_0) = \sum_{n=0}^{\infty} A^{(n)}_m \exp\left(\frac{-n(n+1)\pi^2 K_i L_i}{4B_i^2 U_i}\right) \hat{\Phi}^{(n)}_{\mu}(x_0, y_0). \tag{8.6}$$

The rapid exponential decay with n implies that to achieve any fixed level of accuracy only a modest number of modes need to be calculated. For example, with a channel length L_i equal to a quarter of the symmetric e-folding length L_e, the $n = 10$ or higher modes will have decayed to e^{-4} or less.

We can characterize an isolated island by the end points x_-, x_+ and by the dividing streamline y_I. Thus a volume fraction $\frac{1}{2}(1+y_I)$ of the water flow enters the lower 1 channel and a volume fraction $\frac{1}{2}(1-y_I)$ enters the upper 2 channel. If the discharge took place far upstream of the island, then the dosage Φ will have become uniform across the river before the island is reached. Consequently, the dosages Φ_1, Φ_2 in the two branches either side of the island will remain constant. So the series (8.2) only comprises the $n = 0$ constant term.

At the exit x_+ from the isolated island the Legendre coefficients have the explicit formulae

$$Q\Phi_1^{(0)} = \tfrac{1}{2}(1+y_I), \quad Q\Phi_2^{(0)} = \tfrac{1}{2}(1-y_I), \tag{8.7a, b}$$

$$Q_0 \hat{\Phi}_1^{(n)} = Q\hat{\Phi}_2^{(n)} = \frac{P_{n+1}(y_I) - P_{n-1}(y_I)}{2(2n+1)}. \tag{8.7c}$$

Figure 3(*a*, *b*) shows contours of $Q_0 \Phi_1$ (i.e. the lower route) for the particular cases

(*a*) $y_I = 0$ and (*b*) $y_I = 0.5$. The tight clustering of the dosage contours at the left-hand side of the figures demarcates the abrupt decrease in dosage from 1 for lower-route water to 0 for upper-route water at the trailing edge of the island (x_+, y_I). The longitudinal axis extends to the right for 3 multiples of the symmetric e-folding distance (7.3), corresponding to about $600B$ downstream of the island. For our reference case of $B = 10$ m, figure 3(*a*, *b*) would extend 6 km beyond the trailing edge of the island. Even at such large distances, the dosage has not yet become well-mixed across the flow (principally because of the P_1 mode with its e-folding distance of $3L_e$). The transverse axis is Y/B. So, in case (*b*), $y_I = \frac{1}{2}$, the trailing edge of the island is located at $Y/B = \frac{1}{3}$. If we require dosage contours $Q\Phi_2$ for the upper route, then it suffices that we replace the contour labelling r by $1-r$.

For later use we record that in figure 3(*b*) the lower-route dosages at the far right on the upper bank, centreline and lower bank are

$$Q\Phi_1 = 0.52, 0.77, 0.93, \tag{8.8}$$

while at the same points the upper-route dosages are

$$Q\Phi_2 = 0.48, 0.23, 0.07. \tag{8.9}$$

Thus, even at large distances downstream, the relative importance of the two routes past the island is quite different at different points across the flow.

9. Elapsed time either side of the island

For the illustrative example of a discharge far upstream of an isolated island, the dosages Φ_1, Φ_2 are constant in the two branches either side of the island. Hence, the effective travel speed along each branch is precisely the bulk velocity U_i for that branch. The elapsed times along the two sides of the island are

$$\tau_i(x_+) - \tau_i(x_-) = L_i/U_i. \tag{9.1}$$

The flux-weighted travel time past the island is

$$\tau(x_+) - \tau(x_-) = \frac{1}{2}\left(\frac{1+y_I}{2}\right)\frac{L_1}{U_1} + \left(\frac{1-y_I}{2}\right)\frac{L_2}{U_2}. \tag{9.2}$$

Relative to the flux-weighted travel time, the travel times along the individual channels are related to the difference in travel times for the two sides of the island

$$\tau_1(x_+) - \tau(x_+) = -\left(\frac{1-y_I}{2}\right)\left(\frac{L_2}{U_2} - \frac{L_1}{U_1}\right), \tag{9.3a}$$

$$\tau_2(x_+) - \tau(x_+) = \left(\frac{1+y_I}{2}\right)\left(\frac{L_2}{U_2} - \frac{L_1}{U_1}\right). \tag{9.3b}$$

Generally we can expect channels with smaller volume flux to have smaller velocities. For example, if the channel lengths are equal, $L_i = L$, the breadths are proportional to the depths, and the eddy transport coefficients scale as the products $H_i U_i$, then the dependence upon y_I is

$$\frac{B_1}{B_0} = \frac{H_1}{H_0} = \left(\frac{1+y_I}{2}\right)^{0.4}, \quad \frac{U_1}{U_0} = \left(\frac{1+y_I}{2}\right)^{0.2}, \quad \frac{K_1}{K_0} = \left(\frac{1+y_I}{2}\right)^{0.6}, \tag{9.4a–c}$$

$$\frac{B_2}{B_0} = \frac{H_2}{H_0} = \left(\frac{1-y_I}{2}\right)^{0.4}, \quad \frac{U_2}{U_0} = \left(\frac{1-y_I}{2}\right)^{0.2}, \quad \frac{K_2}{K_0} = \left(\frac{1-y_I}{2}\right)^{0.6}. \tag{9.4d–f}$$

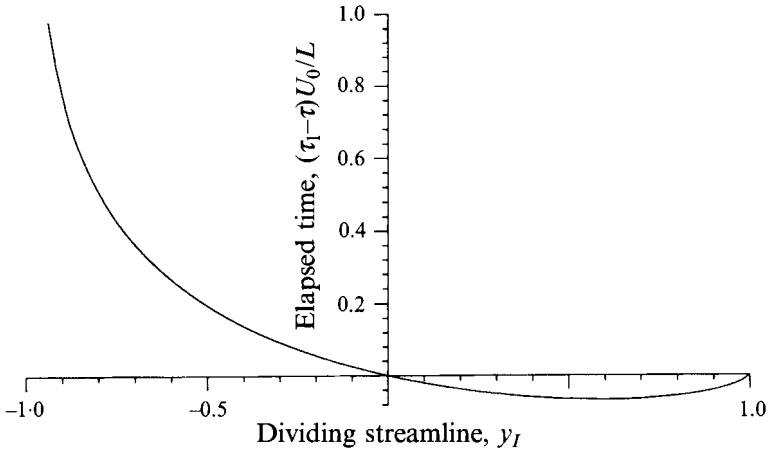

FIGURE 4. Dimensionless time displacement going past an island for the lower 1 route.

The corresponding scalings for the time differences (9.3*a*, *b*) are

$$[\tau_1(x_+)-\tau(x_+)]\frac{U_0}{L}=-\left(\frac{1-y_I}{2}\right)^{0.8}+\left(\frac{1-y_I}{2}\right)\left(\frac{2}{1+y_I}\right)^{0.2}, \tag{9.5a}$$

$$[\tau_2(x_+)-\tau(x_+)]\frac{U_0}{L}=\left(\frac{1+y_I}{2}\right)\left(\frac{2}{1-y_I}\right)^{0.2}-\left(\frac{1+y_I}{2}\right)^{0.8}. \tag{9.5b}$$

Figure 4 shows how the dimensionless time difference for the lower 1 route depends upon the parameter y_I. When y_I is negative and slowly moving water traverses the smaller lower route there is late arrival and positive relative travel time. Conversely, positive values of y_I and rapidly moving water traversing the larger lower route yields early arrival and negative relative travel time. The results for the upper route can be obtained by replacing y_I by $-y_I$.

For later use we note that when $y_I = 0.5$, the dimensionless time differences for the alternative routes either side of the island are

$$-0.065 \quad \text{and} \quad 0.195. \tag{9.6}$$

Thus, for an extremely long island of length $L = 3L_e$, the time difference between the routes would be 0.78 times the e-folding time L_e/U_0 for the downstream channel. If in our reference case $B = 10$ m we also specify the flow speed $U_0 = 0.55\ \mathrm{m\,s^{-1}}$ (winter flow in the Trent), then the time difference becomes 0.78 hours for an island both sides of which have length 6 km.

10. Effective speed downstream of the island

For the cosine velocity and diffusivity profiles (7.5*a–c*) the formulae (5.3*b*) for the slowness can be written

$$\frac{\mathscr{U}}{\mathscr{U}_\mu}=\int_{-1}^{1}\frac{(\Phi_\mu/\Phi_\mu^{(0)})}{\pi(1-y^2)^{1/2}}\,\mathrm{d}y. \tag{10.1}$$

The denominator in the integrand is that conventionally associated with Tchebyshev polynomial expansions, yet the result (8.2) for Φ_μ involves Legendre polynomials.

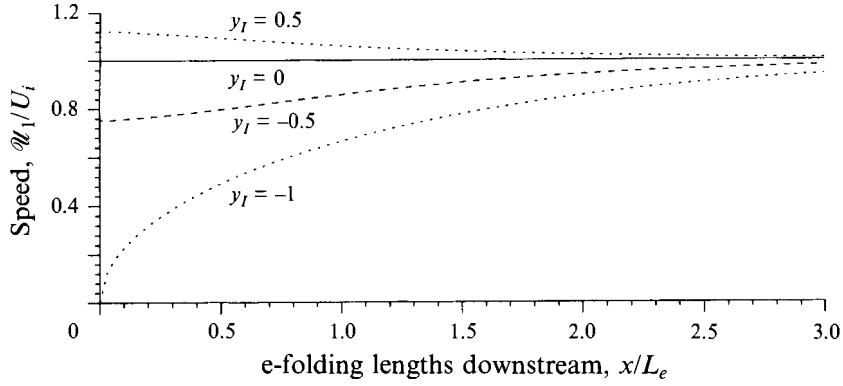

FIGURE 5. Effective speed of tracer downstream of an island for the lower 1 route.

Fortunately, there is a simple link between the two families of polynomials (Erdelyi *et al.* 1954, 10.10.17):

$$P_{2N}(y) = g_N^2 + \sum_{j=1}^{N} g_{N-J}\, g_{N+J}\, T_{2J}(y), \tag{10.2a}$$

$$P_{2N+1}(y) = 2 \sum_{J=0}^{N} g_{N-J}\, g_{N+J+1}\, T_{2J+1}(y), \tag{10.2b}$$

where

$$g_0 = 1, \quad g_{M+1} = \frac{M+\frac{1}{2}}{M+1} g_M, \tag{10.3a, b}$$

or equivalently

$$g_M = \frac{(2M)!}{4^M (M!)^2}. \tag{10.3c}$$

Only the zero-degree Tchebyshev polynomial $T_0 = 1$ contributes to the integral (10.1). Hence, the Legendre series (8.2) for Φ_μ yields a series for the slowness:

$$\frac{U}{\mathscr{U}_\mu} = 1 + \sum_{N=1}^{\infty} (4N+1) g_N^2 \frac{\hat{\Phi}_\mu^{(2N)}}{\Phi_\mu^{(2)}} \exp\left(-N(2N+1)\frac{(x-\hat{x})}{3L_e}\right). \tag{10.4}$$

For the illustrative example of a discharge far upstream of an isolated island the dosages Φ_1, Φ_2 downstream of the island have the Legendre coefficients stated in (8.7*a*, *b*). Figure 5 shows the downstream evolution of the speed $\mathscr{U}_1$ for the tracer which has traversed the lower 1 route. When y_I is negative, the water from the lower channel is subsequently in the slower-moving near-bank region. Hence, the effective speed $\mathscr{U}_1$ is initially small. Conversely, when y_I is positive, the fastest-moving central water originated from the lower 1 channel and the effective speed $\mathscr{U}_1$ is initially large. The slowness only involves the even modes, so the approach to the asymptote is much more rapid than was exhibited by the dosage. To obtain results for the upper 2 route it suffices to replace y_I by $-y_I$.

The elapsed time between $\hat{x}$ and x differs from travel at the bulk velocity $\mathscr{U}_i$:

$$\tau_\mu(x; x_0, y_0) - \tau_\mu(\hat{x}; x_0, y_0) - \frac{m_1}{U_i}(x-\hat{x})$$
$$= \frac{4B_i^2}{\pi^2 K_i} \sum_{N=1}^{\infty} \left[1 - \exp\left(-\frac{N(2N+1)(x-\hat{x})}{3L_e}\right)\right] \frac{g_N^2(4N+1)}{2N(2N+1)} \frac{\hat{\Phi}_\mu^{(2N)}}{\Phi_\mu^{(0)}}. \tag{10.5}$$

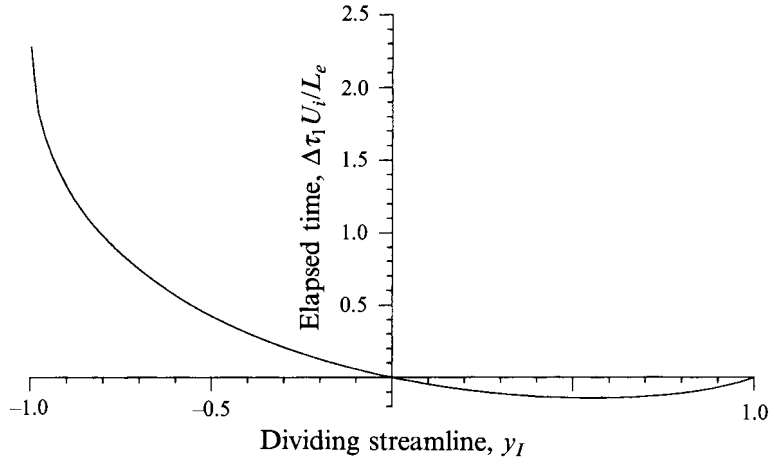

FIGURE 6. Additional time displacement in the adjustment downstream of an island for the lower 1 route.

If the ith channel extends several e-folding distances downstream, then we can characterize the far-field effect of the starting conditions $\Phi_\mu^{(n)}$ in terms of the eventual time displacement

$$\Delta\tau_\mu(\hat{x}; x_0, y_0) = \frac{L_e}{U_i} 6 \sum_{N=1}^{\infty} \frac{g_N^2(4N+1)}{2N(2N+1)} \frac{\hat{\Phi}_\mu^{(2N)}}{\Phi_\mu^{(0)}}. \tag{10.6}$$

Here, the e-folding distance L_e divided by the bulk velocity U_i gives a convenient and physically meaningful non-dimensionalization.

For our standard illustrative example of a discharge far upstream of an isolated island we can use the Legendre coefficients (8.7a, b). Figure 6 shows the asymptotic dimensionless time displacement $\Delta\tau_1 U_i/L_e$ as a function of the island position across the flow y_I. In keeping with the results shown in figure 5, there is a time delay when y_I is negative and water from the lower 1 route moves relatively slowly. The magnitude of the delay can be as large as 2.3 times the travel time over an e-folding distance.

When $y_I = 0.5$ the asymptotic dimensionless time displacements for the alternative routes either side of the island are

$$-0.15 \quad \text{and} \quad 0.45. \tag{10.7}$$

Thus the time difference of 0.6 e-folding times is comparable with the contribution estimated at the end of the previous section in this paper. In our reference case $B = 10$ m, $U_0 = 0.55$ m s^{-1}, the time displacements can be regarded as being in units of hours.

11. Time of arrival

At different positions y across the channel the precise time of arrival will differ from the reference time-of-travel $\tau_\mu(x; x_0, y_0)$. Far downstream within a channel the asymptotic time-of-arrival function G^∞ has the Legendre series representation

$$G^\infty(y) = 6\frac{L_e}{U_i} \sum_{N=1}^{\infty} \frac{g_N^2(4N+1)}{2N(2N+1)} P_{2N}(y). \tag{11.1}$$

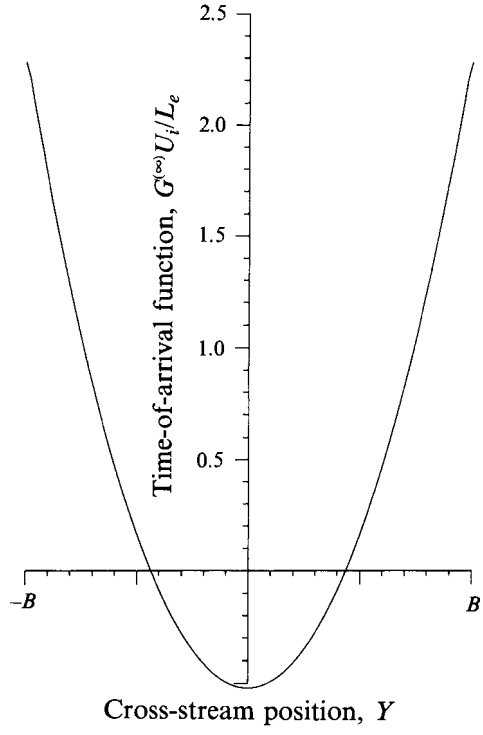

FIGURE 7. Time-of-arrival function far downstream along a channel as a function of observation position Y.

Figure 7 shows a graph of $G^{(\infty)}U_i/L_e$ as a function of the distance Y from the centre of the flow. The temporal centroid occurs slightly earlier in the fast-moving fluid near the centre of the river and substantially later in the slow-moving fluid near the banks.

By analogy with the Legendre series expansion (8.2) for the dosage Φ_μ, we seek to represent $\Phi_\mu G_\mu$:

$$\Phi_\mu G_\mu = \sum_{n=0}^{\infty} (2n+1)\, P_n(y)\, \Gamma_\mu^{(n)}(x; x_0, y_0). \tag{11.2}$$

The P_n component of the field equation (5.2a) yields an ordinary differential equation for $\Gamma_\mu^{(n)}$:

$$\frac{\mathrm{d}}{\mathrm{d}x}\Gamma_\mu^{(n)} + \frac{n(n+1)}{6L_e}\Gamma_\mu^{(n)} = \frac{1}{U}\int_{-1}^{1} \frac{\Phi_\mu P_n(y)}{\pi(1-y^2)^{1/2}}\,\mathrm{d}y - \frac{\hat{\phi}_\mu^{(n)}}{\mathscr{U}_\mu}\exp\left(-\frac{n(n+1)}{6L_e}(x-\hat{x})\right). \tag{11.3}$$

Continuity of $\Phi_\mu G_\mu$ across junctions is ensured by starting conditions:

$$\Gamma^{(n)} = 0 \quad \text{at the discharge } x = x_0, \tag{11.4a}$$

$$\Gamma_{\mu_*}^{(m)} = \sum_{n=0}^{\infty} A_m^{(n)} \Gamma_\mu^{(n)} \text{ across the junction } x = x_*. \tag{11.4b}$$

(We recall that μ_* is the downstream extension of the route μ.)

By construction, $\mathscr{U}_\mu$ has been selected so that $\Gamma_\mu^{(0)}$ exhibits no systematic growth. Hence, $\Gamma_\mu^{(0)}$ retains the value $\hat{\Gamma}_\mu^{(0)}$ transferred across the junction $x = \hat{x}$:

$$[G_\mu]_\mu = \Gamma_\mu^{(0)}(x; x_0, y_0) = \hat{\Gamma}_\mu^{(0)}(x_0, y_0) \quad \text{for} \quad x > \hat{x}. \tag{11.5}$$

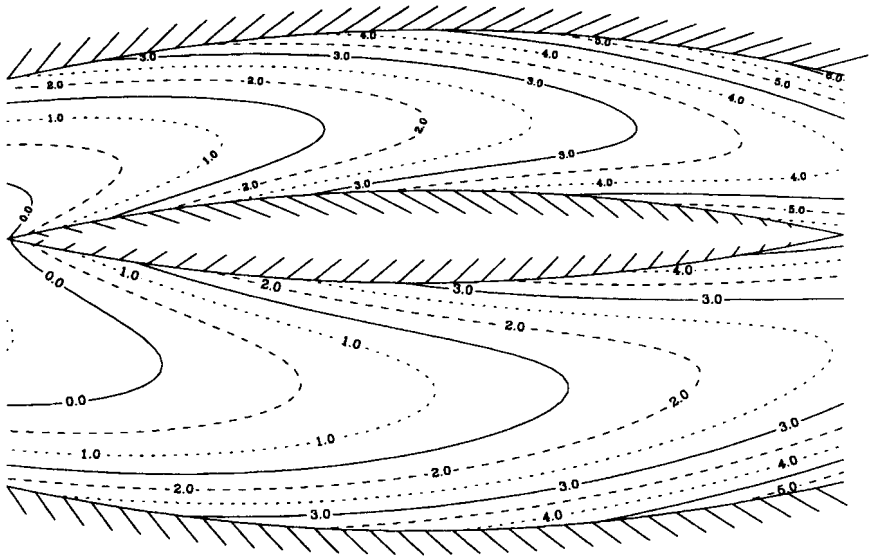

FIGURE 8. Contours of the temporal centroid on both sides of an island, when a quarter of the total flow goes along the upper 2 route. As before there is a foreshortening by a factor of about 100.

If a distributary (sub-channel) receives relatively slow-moving water with G_μ positive, then the continuity of $\Phi_\mu G_\mu$ necessarily requires that on average the downstream value of $\Phi_{\mu_*} G_{\mu_*}$ continues to be positive. The upstream–downstream symmetry of the flow geometry considered here makes $[G_1]_1$ the same as $\Delta\tau_1$ in figure 6. In particular, when $y_J = 0.5$ there will be a time difference of 0.6 e-folding times between the mean entry time for the alternative routes either side of the island.

To evaluate the integral term in (11.3) for $n > 0$ we again use the Tchebyshev representations (10.2*a*, *b*). We define the quantities

$$I_{m,n} = \int_{-1}^{1} \frac{P_m(y)\,P_n(y)}{\pi(1-y^2)^{1/2}}\,\mathrm{d}y. \tag{11.6}$$

It is easy to show that

$$I_{2M,2N} = g_M^2 g_N^2 + 2 \sum_{J=1}^{\min(M,N)} g_{M-J}\, g_{M+J}\, g_{N-J}\, g_{N+J}, \tag{11.7a}$$

$$I_{2M+1,2N+1} = 2 \sum_{J=0}^{\min(M,N)} g_{M-J}\, g_{M+J+1}\, g_{N-J}\, g_{N+J+1}, \tag{11.7b}$$

$$I_{2M,2N+1} = 0. \tag{11.7c}$$

The solution for $\Gamma_\mu^{(n)}$ has the cumbersome form

$$\begin{aligned}\Gamma_\mu^{(n)}(x;x_0,y_0) = {} & \hat{\Gamma}_\mu^{(n)} E_n(x-\hat{x}) - \hat{\Phi}_\mu^{(n)}(1-(2n+1)\,I_{n,n})\frac{(x-\hat{x})}{U}E_n(x-\hat{x}) \\ & + \frac{6L_e}{U}\sum_{\substack{m=0\\ m\neq n}}^{\infty}(2m+1)\frac{\hat{\Phi}_\mu^{(m)} I_{m,n}}{(m-n)(m+n+1)}\{E_n(x-\hat{x}) - E_m(x-\hat{x})\} \\ & - \frac{6L_e}{U}\frac{\hat{\Phi}_\mu^{(n)}}{\Phi_\mu^{(0)}}E_n(x-\hat{x})\sum_{m=1}^{\infty}(2m+1)\frac{\Phi_\mu^{(m)} I_{m,0}}{m(m+1)}\{1-E_m(x-\hat{x})\},\end{aligned} \tag{11.8a}$$

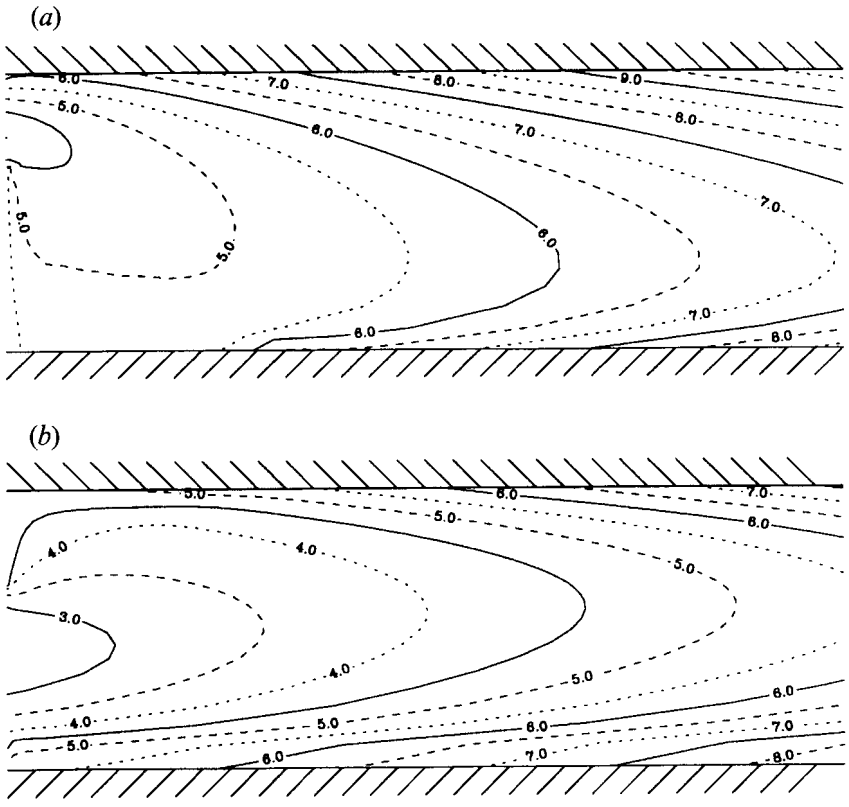

FIGURE 9. Contours of the temporal centroid downstream of an island: (*a*) upper route, (*b*) lower route. Again there is a foreshortening by a factor of about 100.

with $$E_m(z) = \exp(-m(m+1)z/6L_e). \tag{11.8b}$$

For n odd all the terms decay downstream (on the length $3L_e$ of the P_1-mode). For n even the $m = 0$ contribution does not decay and agrees with the far-downstream asymptote (11.1).

As an illustrative example, figure 8 shows the contours of the temporal centroid $\tau_\mu + G_\mu$ either side of a long island when the dividing streamline is at $y_I = 0.5$. (Strictly, the value of the arrival time τ at the island should be added to the contour values.) As in figure 3(*a*, *b*) there is foreshortening by a factor of about 100. The relative breadths, velocities and diffusivities within the channels are specified as in (9.4*a–f*). Thus, instead of the 3 (symmetric) e-folding lengths as shown in figure 3(*a*, *b*) there are 3.36 and 5.42 e-folding lengths respectively for the lower 1 and upper 2 channels. The numerical labelling of the contours is in e-folding times relative to the flow in the full-width channels before and after the island. The centroid displacement function in the parent channel is sliced by the island. The initial asymmetry decays and the time-of-arrival function G_μ re-establishes the symmetric shape (11.1) across each of the channels. The initial time difference of 0.6 e-folding times at entry grows to 1.4 e-folding times at exit. For the reference case $B = 10$ m the island would be 6 km long.

Figure 9(*a*, *b*) extends the temporal centroid contours to downstream of the island for (*a*) the upper and (*b*) lower routes. Although the shape of the contours eventually recovers the symmetric shape (11.1), there is a substantial time disparity between the two routes as evidenced in the numerical labelling of the time contours. At the far right

in figure 9(*a*) the dimensionless times of arrival on the upper bank, centreline and lower bank are

$$10.3, \quad 7.2, \quad 8.6, \tag{11.9a}$$

while the lower-route dimensionless times in figure 9(*b*) are

$$7.6, \quad 5.4, \quad 8.4. \tag{11.9b}$$

(Again, the value of the arrival time τ at the island should be added to these times.) In our reference case $B = 10$ m, $U_0 = 0.55$ m s^{-1}, the times can be regarded as being in units of hours.

12. Size of the tracer cloud

Prior to the splitting of the flow at the isolated island the dosage Φ has become uniform and the time-of-arrival function G^∞ has the Legendre series (11.1). Hence, the integral expression (6.3) for the downstream growth of the temporal variance $[\sigma^2]$ can be evaluated:

$$\frac{1}{2}\frac{\mathrm{d}[\sigma^2]}{\mathrm{d}x} = \frac{6L_e}{U^2}\sum_{N=1}^{\infty} g_N^4 \frac{(4N+1)}{2N(2N+1)} = 0.4048\frac{L_e}{U^2}. \tag{12.1}$$

Equivalently, the shear dispersion coefficient has the value

$$\mathscr{D}^\infty = 0.02734\, B^2U^2/K, \tag{12.2}$$

with the inverse dependence upon the transverse diffusion coefficient K that was first revealed by Taylor (1953).

Along the two sides of the island Φ remains uniform and the time-of-arrival function G_μ again has a Legendre series (11.2). Thus, the growth of the temporal variance has the series expansion

$$\frac{1}{2}\frac{\mathrm{d}[\sigma_\mu^2]_\mu}{\mathrm{d}x} = \frac{L_e}{6U_i^2}\sum_{n=1}^{\infty}(2n+1)n(n+1)\left(\frac{\Gamma_\mu^{(n)}}{\Phi_\mu^{(0)}}\right)^2. \tag{12.3}$$

Figure 10 shows the downstream evolution of the temporal dispersion coefficient for the lower 1 route along the island. As before, replacing y_I by $-y_I$ gives the results for the upper 2 route. The physical quantities are assumed to vary with y_I according to (9.4*a–f*). In particular, the quotient U_i^2/L_e is independent of y_I are there is little difference between the growth rates of σ_μ^2 for the alternative routes either side of the island (e.g. the $y_I = -0.5$ and $y_I = 0.5$ curves are close together). The initially small temporal dispersion coefficient can be attributed to the lower κ-values in the narrower channels alongside the island.

Downstream of the island Φ is non-uniform and to evaluate the growth rate of σ_μ^2 we utilize the expression (6.5*a*):

$$\left(\frac{U^2}{2L}\right)\frac{\mathrm{d}}{\mathrm{d}x}[\sigma_\mu^2]_\mu = \sum_{N=1}^{\infty} g_N^2(4N+1)\frac{\Gamma_\mu^{(2N)}}{\Phi_\mu^{(0)}} - \frac{L_e}{4}\frac{\mathrm{d}}{\mathrm{d}x}\int_{-1}^{1}\left(\frac{\Phi_\mu}{\Phi_\mu^{(0)}}\right)\left(\frac{L_e}{U}G_\mu\right)^2 \mathrm{d}y. \tag{12.4}$$

Figure 11 gives the numerical results for the particular case $y_I = 0.5$. As in figure 10, there is little difference between the growth rates of $[\sigma_\mu^2]_\mu$ for the alternative routes either side of the island. The initially large temporal dispersion coefficient can be attributed to the higher κ-values in the faster-moving flow downstream of the island. The diffusive adjustment of $\partial_y G_\mu$ gives a rapid drop in shear dispersion, followed by a gradual recovery towards the asymptote (12.1).

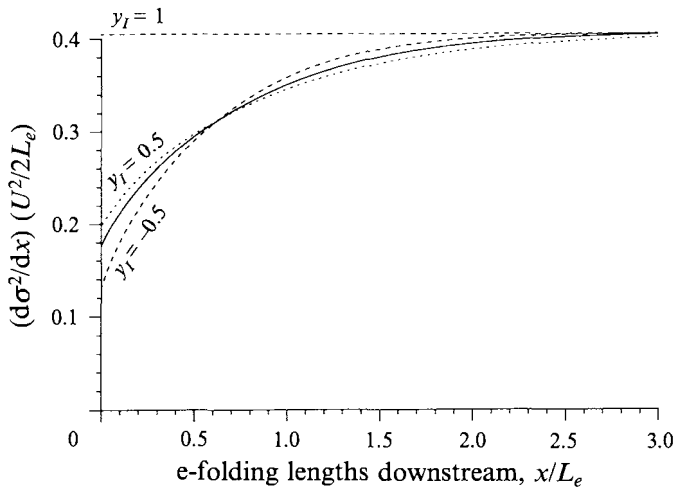

FIGURE 10. Temporal dispersion coefficient for the lower 1 route. The downstream e-folding distance is that for the full-size case $y_I = 1$.

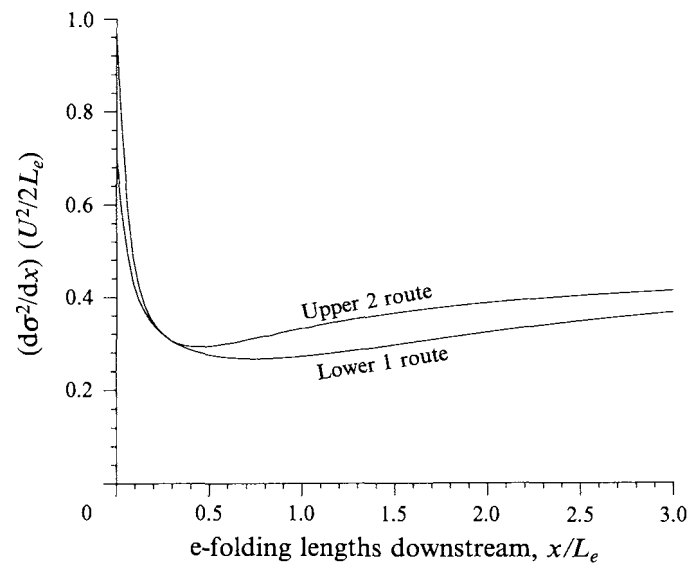

FIGURE 11. Temporal dispersion coefficient downstream of an island for the alternative routes.

For a discharge 3 mixing lengths upstream of the island, the dimensionless temporal variance $[\sigma^2](U/L_e)^2$ at the start of the island would be about 1.2. The precise value would depend upon the source location y_0 across the flow. From figure 10 we can ascertain that going along the island the dimensionless variance would be increased by about the same amount 2.1 for either route. From figure 11 the dimensionless variance 3 mixing lengths downstream of the islands grows by a further 2.2 for the upper route and 1.9 for the lower route. Hence, the total dimensionless temporal variance $[\sigma^2_{\mu}]_{\mu}(U/L_e)^2$ experienced 3 mixing lengths downstream of the island for the two routes would be

$$5.5 \quad \text{and} \quad 5.2. \qquad (12.5a, b)$$

In our reference case $B = 10$ m, $U_0 = 0.55$ m s^{-1}, the temporal variances can be regarded as being in units of hours squared.

13. Tilted Gaussian approximation

The complexity of the calculations escalates rapidly as we proceed to higher temporal moments. For the dosage there was an explicit series (8.2). For the time-of-arrival function G_μ a double series (11.2), (11.8) was used. Finally, the weighted-average temporal variance $[\sigma_\mu^2]_\mu$ needed a numerical integration. Fortunately, at this stage it is possible to construct a Gaussian approximation with respect to t for the concentration.

For spatially uniform flows the Taylor (1953) model for shear dispersion yields instead a Gaussian profile with respect to x. Smith (1987) showed that in an (x, t)-plane, moments can be calculated along any sloping line. The Gaussian approximation is best at a particular non-zero tilt at which the third moment is asymptotically zero. At a fixed value of x or t the best approximation is a 'tilted' Gaussian with respect to the free coordinate.

In the present context the tilted Gaussian approximations compatible with the known temporal moments can be written

$$c_\mu = 0 \quad \text{for} \quad t - t_0 < T_\mu < \tau_\mu, \tag{13.1a}$$

$$c_\mu = \frac{q\Phi_\mu}{(2\pi\Delta_\mu(t-t_0-T_\mu))^{1/2}} \exp\left(-\frac{(t-t_0-\tau_\mu-G_\mu+\Delta_\mu)^2}{2\Delta_\mu(t-t_0-T_\mu)}\right), \tag{13.1b}$$

with

$$\Delta_\mu = \{[\sigma_\mu^2]_\mu + \tfrac{1}{4}(\tau_\mu - T_\mu)^2\}^{1/2} - \tfrac{1}{2}(\tau_\mu - T_\mu). \tag{13.1c}$$

The spatial Gaussian solution corresponds to a zero value for the minimum time of travel $T_\mu(x; x_0)$.

Chatwin (1980, Appendix A) gives an ingenious method for evaluating temporal moments for such tilted Gaussians. For the approximation (13.1*a–c*) the first few centred temporal moments are

$$\int_{-\infty}^{\infty} c_\mu \, \mathrm{d}t = q\Phi_\mu, \quad \int_{-\infty}^{\infty} (t - t_0 - \tau_\mu - G_\mu)\, c_\mu \, \mathrm{d}t = 0, \tag{13.2a, b}$$

$$\int_{-\infty}^{\infty} (t - t_0 - \tau_\mu - G_\mu)^2 c_\mu \, \mathrm{d}t = q[\sigma_\mu^2]_\mu \Phi_\mu + q\Delta_\mu \Phi_\mu G_\mu, \tag{13.2c}$$

$$\int_{-\infty}^{\infty} (t - t_0 - \tau_\mu - G_\mu)^3 c_\mu \, \mathrm{d}t = q(3[\sigma_\mu^2]_\mu + 2\Delta_\mu^2)\Delta_\mu \Phi_\mu + 3q\Delta_\mu^2 \Phi_\mu G_\mu, \tag{13.2d}$$

where

$$[\Phi_\mu G_\mu]_\mu = 0. \tag{13.2e}$$

Hence, the tilted Gaussian approximation exactly replicates the zero and first moments. When averaged across the flow, the second moment is likewise correct. If the cross-flow average of the third moment were known (Smith 1984), then it would be possible to select optimally the effective minimum time of travel $T_\mu(x; x_0)$.

An elementary way of estimating T_μ is to use the peak flow speed along the route μ. For example, a tracer released at time $-3(L_e/U)$ at a distance $3L_e$ upstream of the island would first reach the island at dimensionless time

$$-3 + 6/\pi \approx -1.1. \tag{13.2}$$

The upper and lower routes alongside the island of length $3L_e$ contribute additional minimum dimensionless travel times

$$2.5 \quad \text{and} \quad 2.0. \tag{13.4a, b}$$

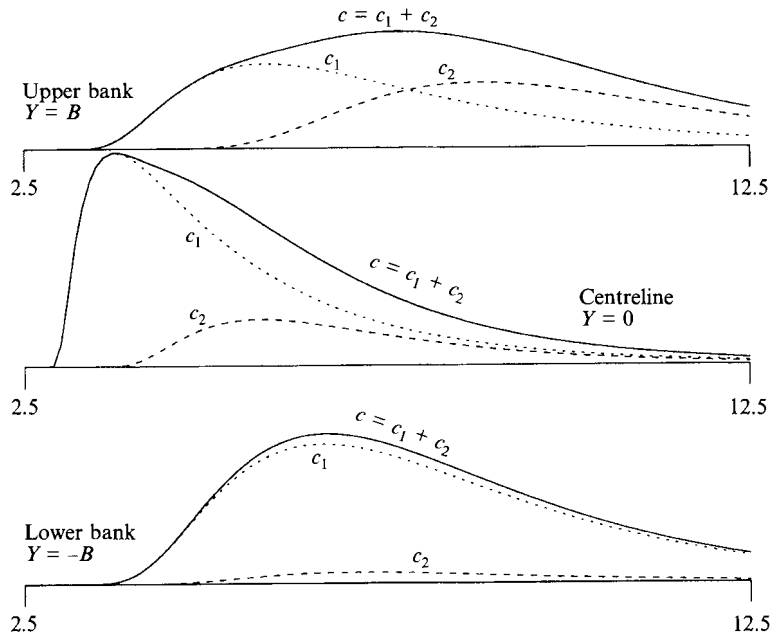

FIGURE 12. Tilted Gaussian approximations for the concentrations as functions of time at the centre and sides 3 e-folding distances downstream of the island.

Downstream of the island the remaining length $3L_e$ takes a further minimum dimensionless time 1.9. Hence, the earliest dimensionless times of arrival via the upper and lower routes are

$$3.3 \quad \text{and} \quad 2.8. \qquad (13.5a, b)$$

By comparison, assuming that the centroid arrival time at the island is zero, the dimensionless centroid times $\tau_\mu(U/L_e)$ at the standard $3L_e$ downstream of the island for the upper and lower routes are

$$7.8 \quad \text{and} \quad 5.9. \qquad (13.6a, b)$$

The results at the standard distance 3 mixing lengths downstream of the island and at the standard cross-channel locations on the upper bank, centreline and lower bank, are scattered throughout the paper: (8.8), (8.9) for the dosages Φ_μ, (13.6a, b) for the reference travel times τ_μ, (11.9a, b) for the composite temporal centroids $\tau_\mu + G_\mu$, (12.5a, b) for the temporal variances σ_μ^2 and (13.5a, b) for the earliest times of arrival T_μ. Combining all these results into the tilted Gaussian approximation (13.1a–c) gives the concentrations c_1 and c_2 shown in figure 12. In our reference case $B = 10$ m, $U_0 = 0.55$ m s^{-1}, the dimensionless time axis in figure 12 can be regarded as being in units of hours after the centroid arrival time at the beginning of the island.

14. Concluding remarks

In figure 12 all the qualitative features discussed in this paper can be seen. The concentrations c_1 and c_2 from the two routes either side of the island have different magnitudes, arrival times and spreads. Also, the magnitudes and arrival times exhibit strong differences at the different locations across the flow. On the upper bank the

upper-route concentration c_2 is of enhanced significance, while on the lower bank the lower-route concentration c_1 dominates. At such large distances (totalling about $1800B$ or in the reference case 18 km) between tracer release and observations, the temporal spread exceeds the temporal separation between the contributions c_1 and c_2. So, the superposition does not exhibit multiple peaks (as would a release close to the start of the island and observed only a short distance downstream of the end of the island). Nevertheless the total concentration (continuous) curves in figure 12 are noticeably different from each other. For example, the total concentration on the upper bank is more dispersed than on the lower bank and the concentration at the centre of the river arrives abruptly and reaches a relatively large maximum value at an early time.

The key assumptions upon which this paper is based are (i) vertically well-mixed flow, (ii) neglect of longitudinal turbulent diffusion, (iii) the concentration can be characterized by the first few moments with respect to time, (iv) steady flow. The first three in that list of assumptions all preclude us from making meaningful predictions for the concentration any closer than several channel breadths downstream of the tracer release site. At shorter distances the calculated shear dispersion associated with the lateral shear of the vertically averaged flow would be growing rapidly but would not yet have dominated the neglected longitudinal shear dispersion associated with the vertical shear and the neglected longitudinal turbulent mixing. The predicted concentrations near the tracer release site would be too large, particularly in the centre of the flow where the lateral shear is zero. However, a lot of river remains in which those three assumptions are reasonable. It is the steady flow assumption (iv) that is the most restrictive. Neither estuarine flows nor sudden flooding events can be studied with the methods developed in this paper.

The central message of this paper, as conveyed in figure 12, is that the complexity of tracer concentrations in multi-connected flows is principally the complexity of superposition. The illustrative example involved just a single very long island. A larger number of islands would imply a larger number of routes $\boldsymbol{\mu}$ and a richer range of possibilities in the superposition of the individual concentration distributions. Each of these contributions evolves along its route $\boldsymbol{\mu}$ in an essentially diffusive (tilted Gaussian) manner and can be quantified in terms of its first few temporal moments.

REFERENCES

ADLER, P. M. 1985 Transport processes in fractals – III. Taylor dispersion in two examples of fractal capillary networks. *Intl J. Multiphase Flow* **11**, 241–254.

ARIS, R. 1956 On the dispersion of a solute in a fluid flowing through a tube. *Proc. R. Soc. Lond.* A **235**, 67–77.

CHATWIN, P. C. 1980 Presentation of longitudinal dispersion data. *J. Hydraul. Div. ASCE* **106**, 71–83.

DAISH, N. C. 1985 Shear dispersion problems in open-channel flows. PhD thesis, Cambridge University.

ERDELYI, A., MAGNUS, W., OBERHETTINGHER, F. & TRICOMI, F. G. 1954 *Higher Transcendental Functions*, vol. II. McGraw Hill.

FISCHER, H. B. 1969 The effect of bends on dispersion in streams. *Water Resources Res.* **5**, 496–506.

FUKUOKA, S. & SAYRE, W. W. 1973 Longitudinal dispersion in sinuous channels. *J. Hydraul. Div. ASCE* **99**, 195–217.

SAFFMAN, P. G. 1969 A mathematical treatment of dispersion in flow through a branching tree. In *Circulatory and Respiratory Mass Transport* (ed. G. E. W. Wolstenholme & J. Knight), pp. 298–301. J & A Churchill Ltd.

SMITH, R. 1981 The importance of discharge siting upon contaminant dispersion in narrow rivers and estuaries. *J. Fluid Mech.* **108**, 43–53.

SMITH, R. 1984 Temporal moments at large distances downstream of contaminant releases in rivers. *J. Fluid Mech.* **140**, 153–174.

SMITH, R. 1987 Shear dispersion looked at from a new angle. *J. Fluid Mech.* **182**, 447–466.

SMITH, R. & DAISH, N. C. 1991 Dispersion far downstream of a river junction. *Phys. Fluids* A **3**, 1102–1109.

TAYLOR, G. I. 1953 Dispersion of soluble matter in solvent flowing slowly through a tube. *Proc. R. Soc. Lond.* A **219**, 186–203.

TSAI, Y. H. & HOLLEY, E. R. 1978 Temporal moments for longitudinal dispersion. *J. Hydraul. Div. ASCE* **104**, 1617–1634.

TSAI, Y. H. & HOLLEY, E. R. 1980 Temporal moments for longitudinal dispersion. *J. Hydraul. Div. ASCE* **106**, 2063–2066.

ULTMAN, J. S. & BLATMAN, H. S. 1977 A compartmental model for the analysis of mixing in tube networks. *AIChE J.* **23**, 169–176.

YOTSUKURA, N. & COBB, E. D. 1972 Transverse diffusion of solutions in natural streams. *US Geol. Survey Paper*, 582-C.

YOTSUKURA, N. & SAYRE, W. W. 1976 Transverse mixing in natural channels. *Water Resources Res.* **12**, 695–704.